European Organization for Nuclear Research
CERN AB Departement

AB-Note-2007-028

Longitudinal and Transverse Wire Measurements for the Evaluation of Impedance Reduction Measures on the MKE Extraction Kickers

T. Kroyer, F. Caspers, E. Gaxiola

Abstract

In 2003 significant heating of the MKE Extraction kicker magnets in CERN's SPS was confirmed by measurements with beam. The dissipated power was so high that it would seriously jeopardize the good functioning of the kicker by warming the ferrite above the Curie temperature. In an impedance reduction campaign the beam coupling impedance of the present kickers was assessed with wire measurements and possible cures were evaluated. For a reliable impedance determination refined measurement methods had to be used. Any kicker modification should not deteriorate kick field quality and high voltage capability. Shielding the ferrites with printed metallic strips turned out to be a promising solution. Technological issues of the metallic coatings are also discussed.

Geneva, Switzerland
June 2007

Contents

Chapter 1

Introduction

Beam coupling impedance is a critical issue in many high intensity particle accelerators. The problems are twofold: longitudinal and transverse impedance may drive instabilities and cause undesired tune shifts, while the real part of the longitudinal impedance also gives rise to power dissipation in the component. For high intensities this may cause significant heating, as was found in the SPS MKE extraction kickers in 2003, when the kickers were heated by about 60° C, approaching the Curie temperature at $\approx 130°$ C. In this temperature range the kicker functionality is impaired; going beyond the Curie temperature mechanical damage is also possible [1].
In many cases a component's beam coupling impedance can be determined using analytical calculation or numerical simulations. In some situations, however, due to complex geometries or not very well known electromagnetic material parameters, these two approaches are difficult and complementary information is desirable. Measurements with beam generally give only an overall picture of the entire machine or at best a coarse localization of elements with high impedance [2]. Additionally, most of such measurements require precious beam time. Wire measurements on the other hand can be done on parts or the entire component in air in the laboratory.
To reduce the real part of the longitudinal impedance to reasonable values an RF bypass has been installed. Additionally, in order to get a better understanding of other intensity limitations the transverse impedance was determined. After a discussion of the measurement techniques used, the modifications on the kickers will be shown together with the results obtained.

Chapter 2

Wire measurement techniques

Wire measurements rely on the fact that the electromagnetic field distribution of an ultrarelativistic beam is very similar to that of a TEM line. Both longitudinal and transverse coupling impedance can be determined by using a single wire or two wires driven in phase opposition. The standard wire measurement techniques are described in [3]. Generally speaking, the wire diameter should be made as small as possible to get a high line impedance, which best reflects the fact that the beam acts as an ideal current source. A practical criterion is that the line impedance should be much higher than the component's impedance. However, with typical line impedances of the order of a few hundred Ohms, this cannot be fulfilled for many accelerator components. Conversely, for very small impedances it can be worthwhile to work with low line impedances, since then the same effects are more easily measurable. The desired small wire diameter also conflicts with the required low losses in the wire.
The measurement device of choice is a two-port vector network analyser. In this chapter the practical issues related to wire measurements will be discussed in some detail, too, starting with sag.

2.1 Sag

For horizontal accelerator elements which are longer than roughly 1 m, the effect of sag may play a significant role. An obvious solution to this problem would be to put the element in a vertical position as done e.g. for certain measurements in superconducting cavities, however, this is not always a practical solution. The sag is given by

$$s = \frac{gl^2}{8H} \tag{2.1}$$

for a wire with a weight force per length g and length l on which a horizontal force H acts. Tension forces of the order of 10 N may be necessary; in case the material of choice, copper, cannot stand the required tension, CuBe can be used. Steel wires should be considered with care, since they have a finite (and frequency-dependent) magnetic permeability.

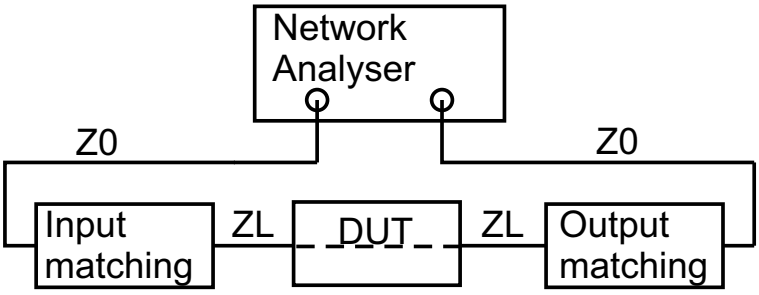

Figure 2.1: The setup for a longitudinal impedance measurement. The DUT line is composed of the DUT itself with the inserted wire.

2.2 Longitudinal measurements

Longitudinal measurements are rather straightforward to perform. A single wire is inserted into the device under test (DUT) and the signal transmission (S_{21}) is measured, from which the longitudinal impedance can be calculated. For small losses a resonant measurement may be a better approach, since very high sensitivity can be obtained this way.

2.2.1 Single wire transmission

The set-up for a single wire measurement is sketched in Fig. 2.1. The generator and the connecting cables are usually devices with $Z_0 = 50\ \Omega$, while the TEM line composed of the wire and the DUT in general has a higher line impedance Z_L. For a circular beam pipe and wire the line impedance is given by the well-known expression [4]

$$Z_L/\Omega = 60 \ln \frac{D}{d} \tag{2.2}$$

with the beam pipe diameter D and the wire diameter d. Approximate formulae are available for other geometries. Another very common case is a flat beam chamber. For a wire between two parallel plates spaced by D

$$Z_L/\Omega = 60 \ln \left(1.27 \frac{D}{d}\right), \tag{2.3}$$

while for a square with side length D the geometric factor in the argument of the logarithm is 1.08. Since most impedance measurements are done over large frequency ranges, a wide band matching is necessary.

Matching. Several techniques exist for matching the line in the DUT to the system impedance Z_0:

- The use of a transformer for not too high frequencies [5, 6].
- Since power loss is not much of an issue, resistive matching is another option. There are two approaches:

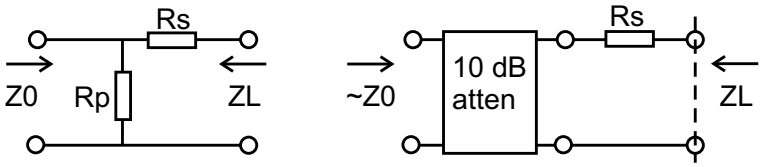

Figure 2.2: Resistive networks for the input matching. Left: Two resistors can be used for full matching. Right: A single series resistor provides one-way matching from the DUT to the measurement system.

  - Two-way matching is possible with two resistors (Fig. 2.2, left). The values of the series and parallel resistor are given by

$$R_p = Z_0 \sqrt{\frac{Z_L}{Z_L - Z_0}}$$
$$R_s = Z_L - \frac{Z_L R_p}{Z_L + R_p}$$

  - One-way matching only from the DUT to Z_0 can be done with a single series resistor (Fig. 2.2, right). In this case we simply have

$$R_s = Z_L - Z_0. \tag{2.4}$$

    The reflections back to the generator are reduced by attenuators. A calibration on the DUT side of the matching network (reference plane indicated by a dashed line in Fig. 2.2) then allows measurements to be made in a system with impedance Z_L. This technique is very fast and handy, but the power dissipation and reflection by the matching resistors and attenuators may impact sensitivity. Care should be taken that the resistors really behave as such over the entire frequency range of interest.

- For high frequencies a tapered coaxial line can be used. This method works well only when the taper is much longer than the wavelength.
- In case a thick wire can be tolerated the line in the DUT can be built with line impedance Z_0, connected to the measurement lines by a taper of constant impedance Z_0.

Impedance evaluation. The transmission across the DUT, $S_{21,DUT}$ is measured and compared to an ideal reference line ($S_{21,REF}$). The response of the reference line can be measured or calculated according to the available analytical models. For instance, $S_{21,REF}$ for a homogeneous matched line corresponds to the electrical length of the DUT. The corrected transmission S_{21} is then given by

$$S_{21} = \frac{S_{21,DUT}}{S_{21,REF}} \tag{2.5}$$

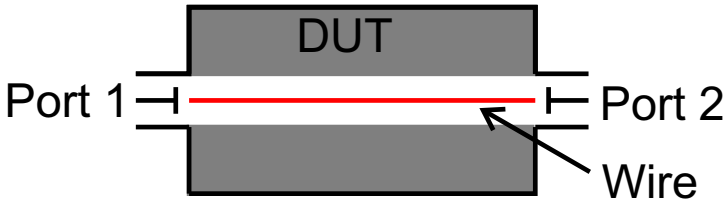

Figure 2.3: The resonator method for measuring the longitudinal impedance allows high sensitivity to be obtained. Capacitive coupling is used on both sides of the structure.

For the calculation of the longitudinal impedance Z a number of formulae involving different approximations exist [3,7,8,9]. The main parameter is the (normalized) electrical DUT length Θ, defined as

$$\Theta = 2\pi \frac{L}{\lambda}, \tag{2.6}$$

where L is the length of the DUT and λ the wavelength. The formulae can be summarized as follows.

- *Lumped impedance formula.* For a short component, where $\Theta \leq 1$ *and* L smaller than the beam pipe diameter the impedance is given by

$$Z = 2Z_L \frac{1 - S_{21}}{S_{21}}. \tag{2.7}$$

  For longer structures this formula may yield unphysical results.

- *Log formula.* For distributed impedances a good approximation is given by

$$Z = -2Z_L \ln S_{21}. \tag{2.8}$$

  This formula is very versatile, it can be also applied for lumped impedances, although it is less accurate in this case.

- *Improved log formula.* For long components and/or high frequencies ($\Theta \geq 1$) a better approximation is given by

$$Z = -2Z_L \ln S_{21} \left(1 + j \frac{\ln S_{21}}{2\Theta}\right). \tag{2.9}$$

  However, contrary to the "standard" log formula it cannot always be used when $\Theta \leq 1$. For instance, for a frequency-independent lumped impedance the term $\ln S_{21}/(2\Theta)$ diverges as $f \to 0$, which is unphysical.

2.2.2 Resonant measurements

When high sensitivity is needed, the transmission technique discussed above may not be sufficient. The TEM line in the DUT can be readily adapted for resonant measurements by replacing the connection of the wire to the inner conductor of the measurement lines by capacitive coupling (Fig. 2.3). The structure resonates when

$$L = n\lambda/2 \tag{2.10}$$

where L is the structure length, λ the wavelength and n the number of the resonance. The resonator method presents several advantages:

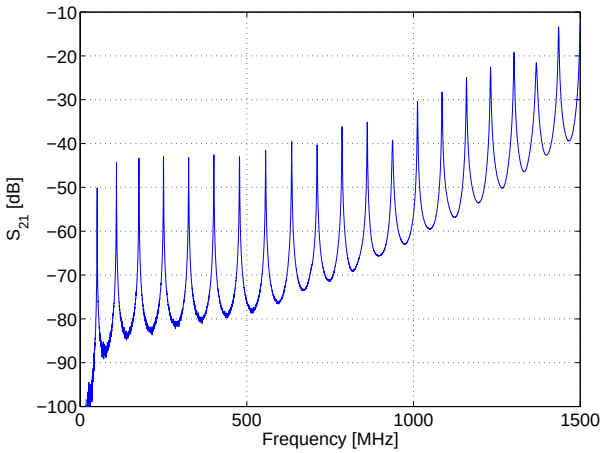

Figure 2.4: Typical pattern found in a resonant measurement of a graphite collimator for LHC. The quality factor of each peak allows the real part of the longitudinal impedance at the respective frequency to be calculated.

- The transmission losses corresponding to the real part of the longitudinal impedance can be measured with a very high precision.
- No matching is needed.
- It is immune to many spurious effects, such as connector repeatability, instrument drift or calibration uncertainties.

However it is to be used with care if the impedance of the DUT changes rapidly with frequency.
In Fig. 2.3 it is also possible to short-circuit port 2. The resonance condition is then

$$L = (2n - 1)\lambda/4. \tag{2.11}$$

However, the quality factor measurement is more difficult in reflection than in transmission.
The quality factor Q of each resonance can be determined to a very high precision and can be used to calculate the line attenuation and thus the real part of the longitudinal impedance. It must be noted that only *resistive* losses show up, while losses due to reflections inside the structure do not (to first order) affect the measured Q. In principle it is also possible to determine the imaginary part of the longitudinal impedance by measuring the detuning of the resonance peaks. However, the coupling elements and other discontinuities in the set-up cause detuning too, thus increasing the uncertainty of the results. A typical resonance pattern is depicted in Fig. 2.4. Due to the frequency-dependency of the capacitive coupling, the absolute magnitude of the first resonance peaks is low. When the coupling is too low, noise starts to affect the measurement, whereas too high coupling introduces an error in the unloaded Q factor determination.

Impedance evaluation. The loaded quality factor Q_L and the magnitude of S_{21} are measured at each resonance peak. In addition, S_{11} and S_{22} can also be recorded,

when a full two-port calibration was done. For weak and approximately equally strong coupling at both ports the coupling coefficient is given by [10]

$$k = \frac{|S_{21}|}{1 - |S_{21}|}. \tag{2.12}$$

The difference between the unloaded Q factor Q_0 and the measured Q_L is of the order of k. An approximate correction can be done by

$$Q_0 = Q_L \cdot (1 + k). \tag{2.13}$$

A better estimation of Q_0 can be inferred by using the reflection coefficients. The measured line attenuation in Np/m is then calculated as [4]

$$\alpha_m = \frac{\pi}{\lambda Q_0}. \tag{2.14}$$

A significant part of the line attenuation may be due to the finite wire resistivity. The wire attenuation can be estimated using the expression for a coaxial line [11]

$$\alpha_w = \sqrt{\pi \rho_w \epsilon f} \frac{1}{d \ln D/d} \tag{2.15}$$

with the wire resistivity ρ_w, the permittivity ϵ, the frequency f, the wire diameter d and the outer conductor diameter D. In addition, at low frequencies the finite skin depth in the inner conductor should be taken into account. Then the real part of the impedance per length is found from the corrected attenuation $\alpha = \alpha_m - \alpha_w$ using the log formula (Eq. 2.8) as

$$\Re\{Z'\} = 2Z_L \cdot \alpha \tag{2.16}$$

where Z_L designates the line impedance in the DUT.

2.3 Transverse measurements

A conventional transverse impedance measurement consists of two wires driven with opposite phases. A dipolar field is excited in the DUT, which interacts with the fringe field only. Therefore the effects are smaller and make the measurements more complicated. For the two wire approximation to hold, the wire spacing should be much smaller than the beam pipe diameter [3,12]. Unfortunately, this conflicts with the practical need to get a clearly measurable effect. A wire spacing of about a third of the aperture appears to be a good compromise. Two wire measurements yield the *detuning* or *dipolar* component of the transverse impedance whereas a moving wire measurement gives the *sum of dipolar and quadrupolar terms* [16].
There are three main methods for the two wire measurement:

- The direct transmission measurement and the resonant loop measurement for rather high frequencies
- The single wire over an image plane
- Ordinary loop measurements below resonance for low frequencies.

The latter method is very well treated in [13,14] and will not be described here. The single wire with image plane suffers from practical problems, since it is not easy to introduce large metal plates into an accelerator component. In addition, waveguide modes may appear in the beam pipe at lower frequencies.

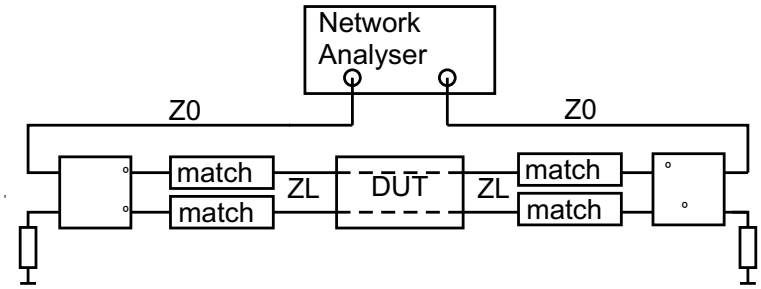

Figure 2.5: Set-up for a transverse impedance measurement. The two wires in the DUT are driven in phase opposition via two hybrids. Each hybrid output is then matched separately to the two-wire line.

2.3.1 Two wire transmission

In practice the phase opposition between the two wires can be obtained by splitting the input signal in a 180° hybrid and recombining it in the same way to get the DUT output signal (Fig. 2.5). Another way would be to use a push-pull transformer. The horizontal/vertical transverse impedance is found when the wires are installed in the horizontal/vertical plane.

Matching. For small wire spacings the beam pipe can be neglected in the calculation of the line impedance. The difference-mode impedance of a two wire line in free space is given as [4]

$$Z_L/\Omega = 120\text{acosh}\frac{\Delta}{d} \tag{2.17}$$

where a is the wire diameter and Δ the spacing.
As for longitudinal measurements one can use a transformer as well as a resistive matching. A transformer with two opposite windings on the secondary side has the advantage of combining the matching and the signal splitting in one element. For resistive matching after a hybrid (Fig. 2.5) each 50 Ω hybrid output has to be matched to half the difference mode line impedance. If matching is done with single series resistors R_S for each wire, the value of each resistor is

$$R_S = Z_L/2 - Z_0. \tag{2.18}$$

Calibration should be done including hybrids and matching networks.

Impedance evaluation. From the measured S_{21} an impedance Z is calculated as in the longitudinal case using Equations 2.7 to 2.9. Then the transverse impedance in the respective plane is found from [13, 3]

$$Z_{TR} = \frac{cZ}{2\pi f\Delta^2}. \tag{2.19}$$

where c is the speed of light. Usually the measured effect is small and the wire attenuation should be removed numerically or by a reference measurement.

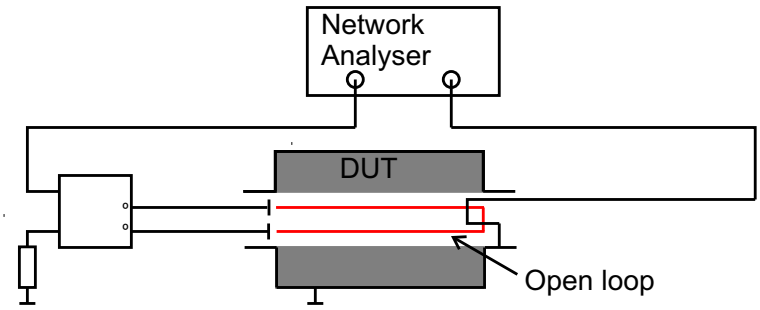

Figure 2.6: Set-up for a resonant transverse impedance measurement. To excite the π mode on the loop, capacitive coupling in phase opposition is used on the open side; on the closed side there is a loop for inductive coupling.

2.3.2 Resonant measurements

The good experience obtained using resonant methods for the longitudinal impedance motivated the search for a similar technique for transverse measurements. In principle two wires can be driven resonantly. With two parallel isolated wires left open on both sides, two resonant modes are possible:

1. The "0" mode: the current has the same phase in both wires. For small wire spacing this corresponds to the single wire measurement.

2. The "π" mode: the current has opposite phase in the two wires. The mode attenuation is related to the transverse impedance.

The two modes are degenerate, which makes them difficult to use in practice. A very good mode-selective excitation would be necessary to suppress the unwanted 0 mode. The same is true for a single loop. However, when an open loop is used, the degeneration is broken.

Resonant loop. An open loop as sketched in Fig. 2.6 can be driven resonantly and can be regarded as a folded $\lambda/2$ resonator. The condition for a π mode resonance is

$$L = (2n - 1)\lambda/4. \tag{2.20}$$

In measurements the 0 mode can be suppressed by mode-selective excitation, i.e. capacitive coupling through a 180° hybrid at the open end and inductive coupling at the shorted end.

Impedance evaluation. The data evaluation went along the same lines as for the longitudinal resonator measurements. From the Q_L and S_{21} of each resonance peak the Q_0 and subsequently the attenuation α_m were calculated. Then α_m was corrected for the wire attenuation and several smaller effects, in particular the finite skin depth at low frequencies, the proximity effect and losses on the shorted side of the loop. In a first test a very good sensitivity was achieved by using 8 mm diameter copper rods. For transverse measurements larger wire radii may be used, since a large line impedance can still be achieved when the wire spacing is large enough. It can be shown that for circular rods the field pattern corresponds to the one of a line with thin wires with a wider spacing [4, 15].

2.3.3 Moving wire

In a symmetric structure a single wire measurement yields a longitudinal impedance Z_m of [16, 12]

$$Z_m = Z + Z_{1x}x^2 + Z_{1y}y^2, \tag{2.21}$$

where Z is the ordinary longitudinal impedance measured in the center, x and y are the horizontal and vertical wire offsets and Z_{1x} and Z_{1y} are frequency-dependent coefficients. They are related to "generalized" transverse impedances Z_x and Z_y by

$$Z_x = Z_{TR,x} - Z^{detuning} = \frac{c}{2\pi f} Z_{1x} \tag{2.22}$$

$$Z_y = Z_{TR,y} + Z^{detuning} = \frac{c}{2\pi f} Z_{1y}. \tag{2.23}$$

Here $Z_{TR,x}$ and $Z_{TR,y}$ designate the usual ("driving") transverse impedances as found in the two-wire measurement. $Z_{TR,x}$ and $Z_{TR,y}$ are linked to a wakefield generated by an on-axis charge on an off-axis test charge. $Z^{detuning}$ is related to the wakefield of an off-axis charge on an off-axis test charge. Taking the sum of these two equations $Z^{detuning}$ can be eliminated, giving

$$Z_x + Z_y = Z_{TR,x} + Z_{TR,y}. \tag{2.24}$$

Therefore the two-wire measurements in both planes can be compared to the moving wire data.
In practice Z_m is measured at several positions in the horizontal and vertical plane. When the offset from the center is small the change in Z_m between individual measurements may become comparable to the measurement uncertainty, while for too large offsets higher-order terms would have to be included into Eq. 2.21. It should be noted that Z_L changes as the wire is moved off-center. This cannot be neglected in general, since the effect may be of the same order as the expected change in Z_m.

Impedance evaluation. For constant offset $y = y_0$ the measured Z_m is a second order polynomial of x. The coefficient Z_{1x} can be extracted by fitting a parabola to the measured data at each frequency point. Similarly, Z_{1y} can be determined by measurements with vertical offset. The sum of the transverse impedances $Z_{TR,x} + Z_{TR,y}$ can be found using Equations 2.23 and 2.24.

2.4 Summary

The determination of the beam coupling impedance by means of wire measurements was discussed focussing on practical aspects. Longitudinal measurements are a rather straightforward technique and several possibilities of impedance matching between the measurement system and the device under test were considered. In addition to ordinary transmission measurements resonant methods can be used. At distinct frequencies they offer high sensitivity and low susceptibility to most spurious effects.
For the transverse impedance the two wire transmission measurement is the standard technique. Also, we presented a novel resonant technique providing high sensitivity in transverse measurements. Furthermore, we discussed the moving wire method, that allows the determination of a sum of the dipolar and quadrupolar terms of the transverse impedance.

Chapter 3

Magnet lay-out

The MKE kickers are fast kickers for extraction of the LHC beam from the SPS towards LHC and towards the CNGS (CERN Neutrinos to Gran Sasso) fixed target. They are built with a U-shaped ferrite yoke, which is excited by a current pulse in a single loop. The cross-section of the kicker is shown in Fig. 3.1. The kickers are composed of seven ferrite cells which are separated by a metallic support structure, see Fig. 3.2. These ferrite cells are housed in a vacuum tank having a total length between flanges of $\approx$ 2.2 m. The aperture varies slightly for the different types; it is 147.7 by 35 mm for the MKE-L and 135 by 32 mm for the MKE-S magnets. The ferrite blocks are made of Ferroxcube 8C11 for most of the magnets; only for MKE-L9 the high Curie temperature ferrite Ferroxcube 4E2 was used [17]. More details about the kickers can be found in [18, 19].

3.1 Shielding techniques

When the beam passes through a component containing magnetic material, the beam-induced magnetic field is concentrated in the ferrite. Since in the frequency range of interest (up to $\approx$ 1 GHz) the ferrite used in the MKE kickers has high polarization losses, the real part of the impedance is high. This leads to power dissipation in the ferrite and therefore to a very significant heating [1]. In addition due to the high ferrite permeability μ together with a considerable permittivity ϵ the wake fields are retarded, which causes the imaginary part of the longitudinal impedance to rise. These two effects impact the transverse impedance, as well.
In order to reduce the longitudinal impedance, the beam-induced magnetic field must be prevented from penetrating the ferrite. The most straightforward approach is to install shielding between the beam and the ferrite that guides the image currents. Such a shielding should fulfil the following requirements:

- It must not short-circuit the high voltage kick pulse.
- It should not significantly damp the kick field and should have a very low impact on the fast magnetic field rise time, i.e. eddy current effect should be minimized. This can be done e.g. by using longitudinal strips.
- Any aperture reduction should be minimized.

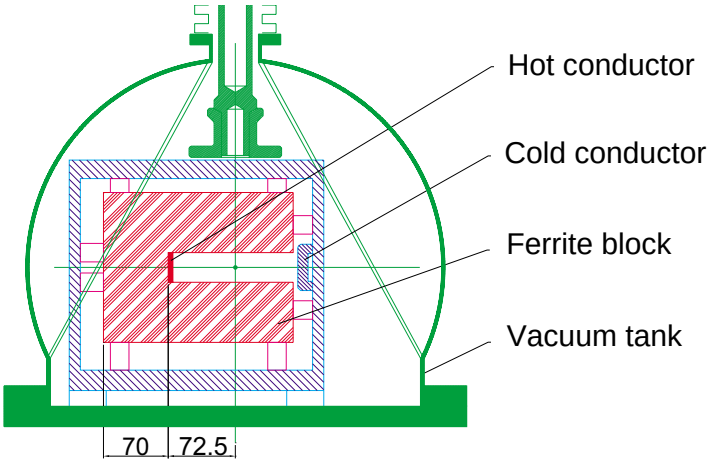

Figure 3.1: Cross-section of the MKE kicker magnet. The beam axis is indicated by the green cross in the center of the aperture. In this structure the high real part of the longitudinal impedance is mainly due to polarization losses in the ferrite close to the beam, which may lead to substantial ferrite heating.

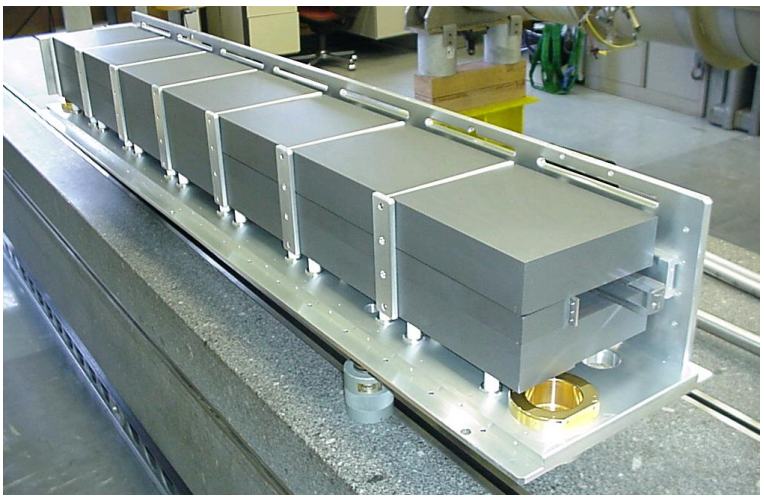

Figure 3.2: An MKE magnet after the assembly of the ferrite cells. The hot and the cold conductor can be seen on the left and right side of the aperture, respectively. In this magnet no shielding is installed, i.e. the beam-induced electromagnetic fields see the “naked” ferrite.

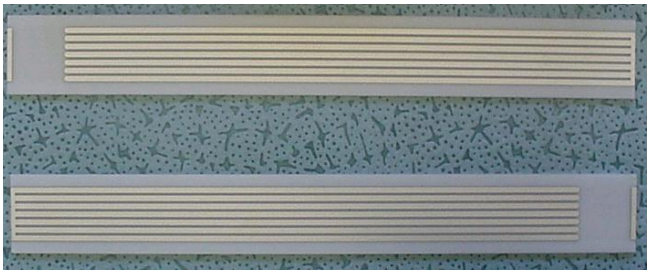

(a) The top and bottom plates of the ceramic insert.

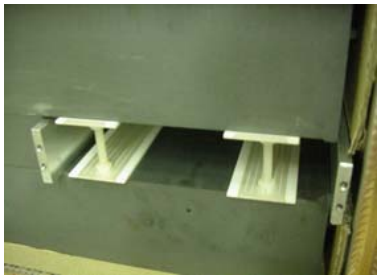

(b) Installation of the ceramic inserts in a single ferrite cell for bench measurements.

Figure 3.3: Ceramic inserts with metallic strips on both sides can be used to shield the ferrite from the beam's electromagnetic fields. The image currents couple capacitively across the dielectric. However, due to aperture restrictions the ceramics can only be installed on the sides of the kicker gap, which reduces the shielding efficiency.

- Ideally it should be possible to retrofit the solution into existing kickers. Therefore the installation should be possible without too large modifications to the kicker, since the available time is very limited.
- The conducting elements should be in good thermal contact with the kicker structure.
- The ultra high vacuum requirements must be respected.

Considering these requirements, two main approaches were identified, namely ceramic inserts with metallic coating on them and metallic strips directly applied onto the ferrite.

3.1.1 Strips on ceramic insert

Since in the MKE kickers the dynamic beam aperture is a flat ellipse there is no beam at the sides of the kicker gap. This allows ceramic inserts to be installed with printed or painted stripes on them in each ferrite cell. The stripes are made from thick film paste; they are electrically connected to the front of the cell on one side and to the back of the cell on the other side. The image currents thus will run along the stripes and capacitively couple across the ceramics. However, the efficiency of this method is limited by the fact that in the center no shielding can be installed without reducing the beam aperture. An implementation of this method is shown in Fig. 3.3. More on the subject, including different ceramic geometries and painted shieldings, is described in [20].

3.1.2 Strips applied directly onto the ferrite

Another option consists of applying low-impedance coatings directly onto the ferrite. Interleaved fingers were realized by painting as well as by serigraphically printing thick-film paste onto the ferrite blocks (Fig. 3.4). A conductor thickness of $\approx 30\ \mu$m after firing was applied with the printing technique, whereas an average thickness of $\approx 200\ \mu$m

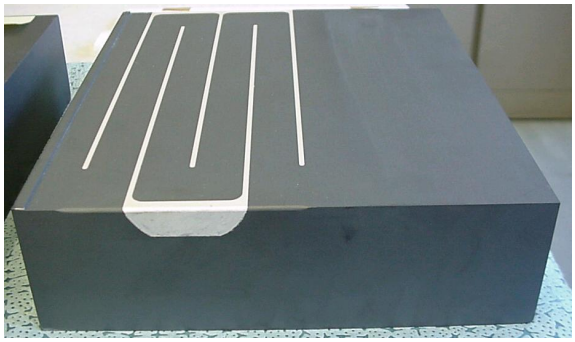

(a) A ferrite block with printed metallic stripes.

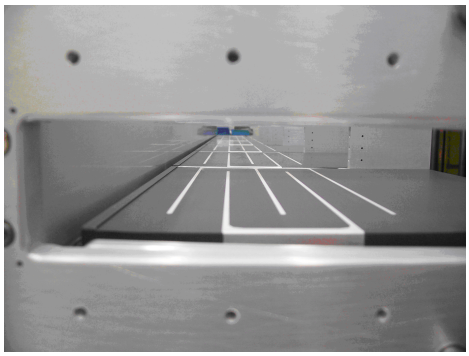

(b) Assembly of the MKE-L10 kicker, which was fully equipped with printed metallic stripes.

Figure 3.4: Interleaved metallic strips directly painted or printed on the ferrite blocks can be used for shielding the entire ferrite surface with negligible aperture loss. The image currents couple capacitively between adjacent strips. Ferrite block length: 205 mm, finger length: 185 mm, finger width: 2 mm, finger spacing: 20 mm.

was found for the painted conductors. Every other finger is connected electrically at the far end of the ferrite block. The geometry was chosen such as to provide a finger spacing sufficient to withstand the high voltage between adjacent fingers while still shielding as much as possible of the ferrite surface. Here the image currents couple capacitively between adjacent fingers. While both painting and printing techniques were tried, printing was retained for various practical reasons; more cost effective and reproducible uniform coating thicknesses could be obtained. In addition, serigraphy yields rounded off conductor edges, which is very convenient for limiting high electrical fields.

3.2 Summary

In order to fight the beam-induced heating of the MKE kickers, a quick and reliable solution for shielding the ferrite blocks was needed. The two main approaches followed were conducting strips on ceramic inserts and interleaved metallic fingers directly applied onto the ferrite surface. Painting and serigraphic printing techniques were used for applying the coatings. After evaluating each technique on single ferrite cells, an entire kicker was equipped with the most promising shielding, which turned out to be serigraphed interleaved fingers. The next chapter is dedicated to the evaluation of the shielding's impact on impedance.

Chapter 4

Longitudinal kicker impedance

During the 2003 scrubbing run in the SPS substantial heating of five MKE type kickers was found [1]. These kickers were equipped with heat conductance ferrite block cooling. Well before that it had been pointed out in several publications that the MKE impedance might be of significant impact on future accelerator performance. [21,22,23]. Finally, at the beginning of 2003 an impedance reduction campaign was started. First, the longitudinal impedance was evaluated on a single ferrite cell and possible ways to reduce it assessed. The principle idea was to provide a low-impedance by-pass for the image currents and thus shield the ferrite from the beam-induced magnetic fields. The latter are responsible for the high observed heating, since they lead to polarization losses in the ferrites. Several options were tested in the single cell for impedance issues. Serigraphed interleaved strips directly on the ferrites were identified as the most promising technique that fulfilled technological, impedance, magnetic field quality and high voltage requirements. A first magnet was fully equipped with this kind of shielding, while two of the other test cells were recuperated from the bench setup and installed as a retrofit at the extremities of another magnet alongside with unshielded ferrites.
For the calculation of Z the standard log formula (Eq. 2.8) was used throughout this report, since it provides a conservative estimate of the kicker impedance and gives useful results in all cases. About 30% higher values may be obtained with the improved log formula, but the latter is difficult to apply in particular at low frequencies and when waves run around the ferrite module inside the kicker tank.

4.1 Tests on a single kicker cell

Given the short timescale and the complexity, cost and effort involved in mounting and demounting entire magnets it was decided to build and measure only single cell prototypes of each shielding option (Fig. 4.1). The results for the entire kicker can then be obtained to a good approximation by scaling to the full length. Uncertainties enter at the following points:

- Without shielding, in a single cell the geometry is homogeneous longitudinally, which is not the case for an entire kicker, since there the cells are separated by metallic high voltage frames.
- In the single cell, the hot conductor was left floating in the test set-up, whereas it is connected and matched to the pulse generator in the fully equipped magnet.

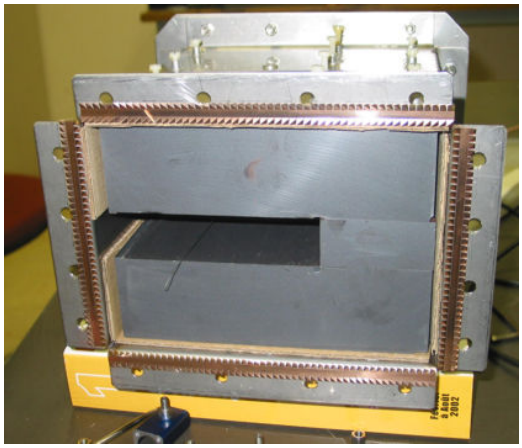

(a) Original geometry: Unshielded ferrites directly seen by the beam.

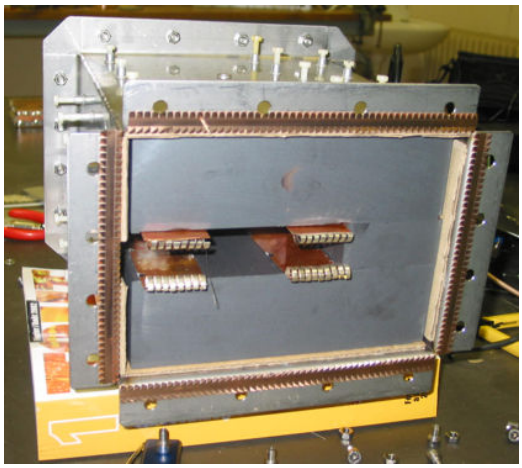

(b) First impedance reduction trial: copper strips on either side of the beam axis.

Figure 4.1: The first step of the impedance reduction campaign: evaluation of the potential improvement on a single ferrite cell. The beam axis is in the center of the aperture.

- Tank modes do not appear in the single cell measurement.

As a first step the effect of ferrite shielding by copper strips was evaluated (Fig. 4.1(b)). The real part of Z for this case is shown in Fig. 4.2 together with the other options. Compared to the unshielded ferrites (black trace) the copper strips (dashed magenta trace) gave a very significant improvement. After this encouraging result it was tried to find solutions that can be used in a real kicker and give a similar impedance reduction. Interleaved fingers printed by serigraphy directly onto the ferrites turned out as the most promising candidate (solid green trace in Fig. 4.2).
For easy comparison and scaling Z was normalised to the length. Below 100 MHz distinct resonances were found. The peak at 66.4 MHz for the unshielded setup should be due to the hot conductor that was left electrically floating inside the cell.

4.2 Impedance reduction with shielding

In this section the longitudinal impedance of two fully assembled magnets is compared, representing the two extreme cases:

1. MKE-L8: no shielding at all
2. MKE-L10: all ferrite cells equipped with serigraphed interleaved metallic stripes

Besides the shielding the two magnets have basically the same geometry.
The raw transmission data is shown in Fig. 4.3(a). The baseline offset of about 15 dB at low frequencies comes from losses in the matching resistors and was removed in the evaluation. An excessive attenuation was found for the kicker without shielded ferrites (black trace). Around 500 MHz S_{21} is below -80 dB and the trace is very ragged. This ruggedness is not due to noise but to an interference of waves going through the ferrite

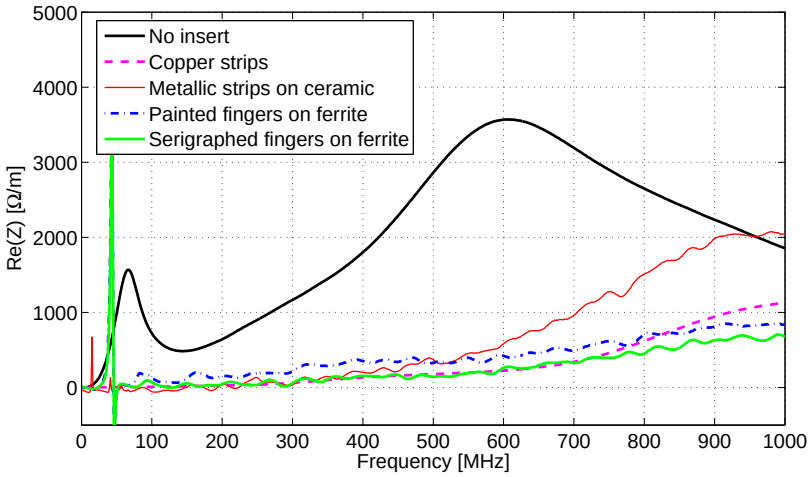

Figure 4.2: Result of longitudinal impedance measurements on a single ferrite cell of 23 cm length. Among the considered options serigraphy fingers on the ferrite gave the largest impedance reduction.

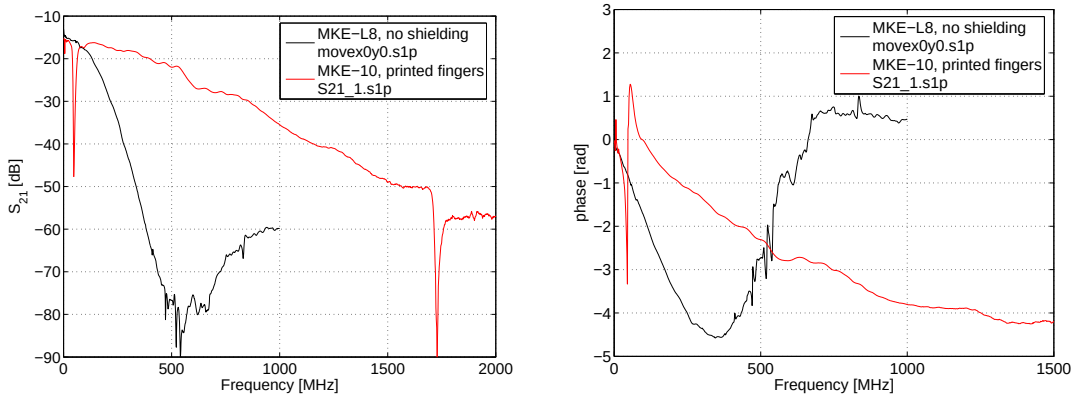

(a) The magnitude transmission is considerably lower for the unshielded kicker.

(b) Below ≈ 500 MHz the phase advance of S_{21} is much larger for the unshielded kicker.

Figure 4.3: Raw wire measurement data for an unshielded and a shielded MKE kicker.

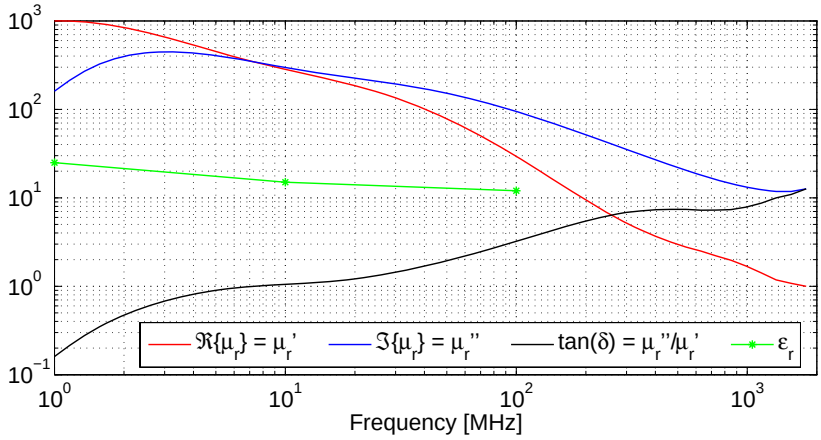

Figure 4.4: The electromagnetic properties of the ferrite type Ferroxcube 8C11 [17].

module and other waves propagating in the space between the ferrite module and the outer kicker tank [21]. The transition piece between the tank and the ferrite module reduces the power coupled to the tank, but it does not eliminate it completely since there are gaps on the sides. The phase of S_{21} has to be considered carefully in this region, since there may be abrupt changes. For the printed fingers the low-frequency resonance previously observed during single-cell measurements was encountered at about 48 MHz. At higher frequencies the curve is smooth, which indicates that the power going through the tank is negligible compared to the power transmitted inside the ferrite blocks.
The origin of the 48 MHz resonance can be explained considering the finger geometry. In the region where the fingers overlap a longitudinal $\lambda/2$ resonance can exist, with electric field maxima at the end of the overlap. Adjacent fingers act like a microstrip line driven in the difference mode. The high permeability μ_r and permittivity ϵ_r of the ferrite causes this resonance to appear at much lower frequencies than in free space. Since the thickness of the ferrite is much larger then the finger spacing and width, the effective permeability and permittivity can be estimated by [24]

$$\mu_{eff} = \frac{\mu_r' + 1}{2}$$
$$\epsilon_{eff} = \frac{\epsilon_r + 1}{2}.$$

For the $\lambda/2$ resonance the resonator length L can be calculated from

$$L = \frac{2nc}{f\sqrt{\mu_{eff}\epsilon_{eff}}} \tag{4.1}$$

where $n = 1$ is the order of the resonance. The high frequency parameters of the used ferrite are given in Fig. 4.4. Evaluating Eq. 4.1 at 48 MHz a resonator length $L = 193$ mm is found, in very good agreement with the 185 mm finger length. Higher order finger resonances are also possible, however due to the strongly frequency-dependent ferrite properties they do not appear at multiples of the fundamental mode. Since μ_r' rolls off fast above 50 MHz these resonances are pushed to much higher frequencies. Numerically solving Eq. 4.1 yields $f \approx 500$ MHz for the second resonance, which corresponds

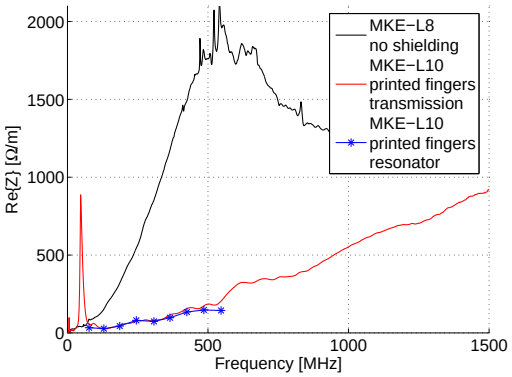

(a) The lower transmission loss with shielding leads to a reduced real part of Z.

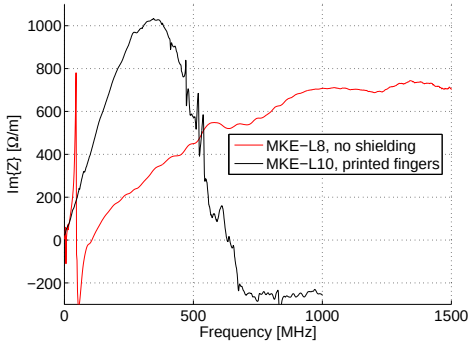

(b) The imaginary part of Z in decreased below 500 MHz.

Figure 4.5: Comparison of the longitudinal MKE impedance with and without shielding.

to the small dip in Fig. 4.3(a) at ≈ 600 MHz. The resonance is strongly damped by the ferrite itself since the loss factor increases quickly with frequency.
Since the 48 MHz resonance is directly linked to the finger length, it can be influenced by changing the finger geometry. For instance, one could try to push this resonance to a higher frequency by shortening the finger overlap. This would move the resonance to a region with higher ferrite losses, which act as an in-built damping. However, decreasing the finger overlap might also degrade the broad-band shielding efficiency. 3D electromagnetic simulations should be used to validate optimized finger geometries.
Fig. 4.5 depicts the Z of both kickers. For easy comparison with other kickers Z was normalized by the tank length of ≈ 2.2 m, a normalization that will also be done for the lost power and transverse impedance. A very important reduction in $\Re\{Z\}$ was obtained. The only drawback is the low-frequency resonance, which fortunately does not fall on a 40 MHz LHC beam harmonic. As a cross-check a resonant measurement was done on the shielded kicker. Excellent agreement between the transmission and resonator data was found (red and blue traces in Fig. 4.5(a)).
The heating power in the magnets was calculated with the measured power spectrum of the LHC type beam in SPS (Fig. 4.6). A substantial reduction, by more than factor four, was found with shielding, for which case a major part of the heating comes from the low-frequency resonance.
Finally, a comparison of the complete MKE kicker inventory is shown in Fig. 4.7.

4.3 Summary

After the confirmation of substantial MKE kicker heating with beam in 2003, an impedance reduction campaign was started. In measurements on a single ferrite cell potential shielding techniques were evaluated. The most promising technique, metallic interleaved fingers printed directly onto the ferrite, was implemented on an entire kicker. A very significant reduction of both the real and imaginary part of Z was found. In terms of heating power with LHC type beam an improvement by a factor four was obtained.

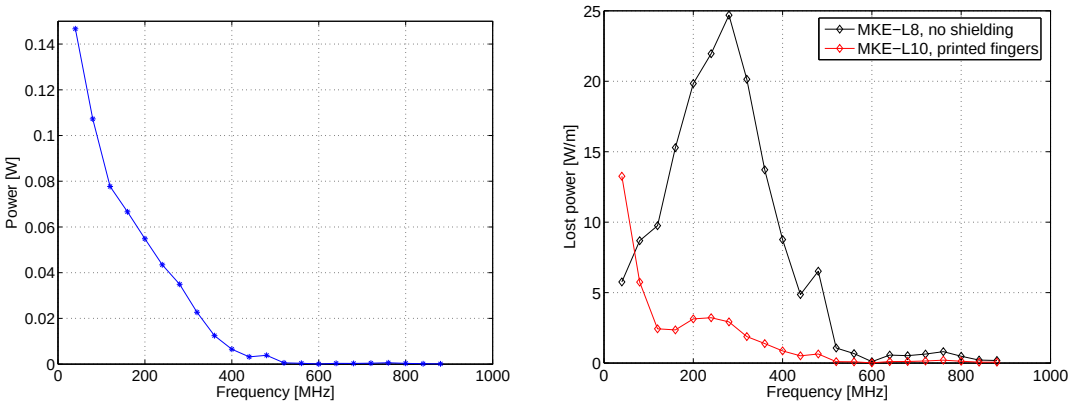

(a) Power spectrum in 1 Ω impedance for the LHC beam at 26 GeV as measured during the 2004 SPS scrubbing run [25].

(b) The total power lost in the kickers for the beam in (a) was reduced by the shielding from 165 W/m to 39 W/m.

Figure 4.6: Calculation of the beam-induced heating power with the measured SPS beam spectrum.

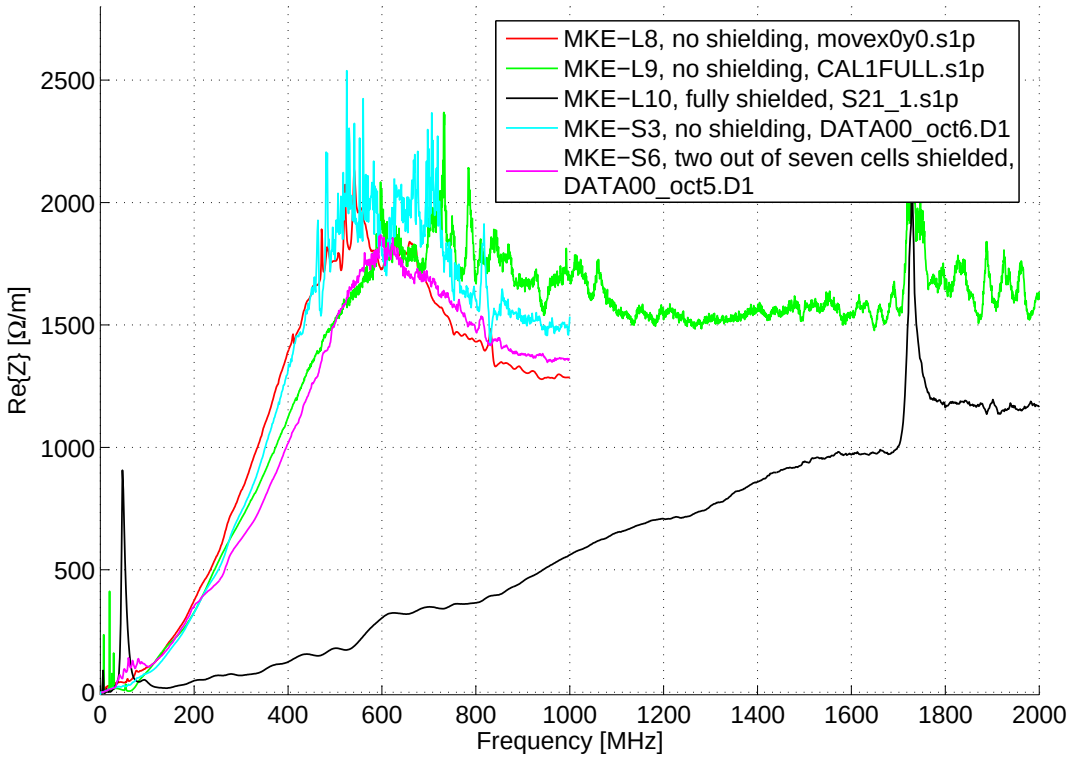

Figure 4.7: Comparison of all types of MKE kickers. MKE-L9 was built with a high Curie temperature ferrite (a lower $\mu_r \approx 25$), MKE-S6 has two ferrite cells equipped with interleaved fingers.

Chapter 5

Transverse kicker impedance

It was found in 2003 with beam measurements that the SPS transverse impedance Z_{TR} had risen by 50% after the re-installation of five MKE kickers [26]. Therefore it was desirable to measure Z_{TR} on a single kicker and to verify, whether the shielding – besides its main purpose of reducing the heating – also has a positive impact on Z_{TR}. A comprehensive measurement programme was carried out on two magnets representing the extreme cases with respect to shielding:

1. MKE-L8: no shielding at all
2. MKE-L10: all ferrite cells equipped with serigraphed interleaved metallic stripes.

The measurements were carried out using the techniques described in section 2.3. All data given is normalized to the tank length of ≈ 2.2 m.

5.1 Two wire measurements

In this section the results of two wire transmission and resonant loop measurements are discussed. Fig. 5.1 shows the results in the horizontal plane. For the real part of Z_{TR} (Fig. 5.1(a)) a very good agreement between transmission and resonant measurements was found. The ripple on the transmission data comes from the residual mismatch between the matching networks and the kicker and from the discontinuity between the kicker tank and the ferrite module. Above 200 MHz a significant decrease of $\Re Z_{TR}$ was found for the shielded kicker, while below there are one or two resonances. As for $\Im Z_{TR}$ again a clear reduction with shielding was found above 100 MHz.

The vertical Z_{TR} is depicted in Fig. 5.2. The agreement between transmission and resonant measurements is not as good as in the horizontal case, which is probably due to sag impacting the wire distance. Again it can be observed that below 200 MHz Z_{TR} is enhanced with shielding, while it is decreased somewhat at higher frequencies. In general the effect of the shielding is less pronounced in the vertical plane.

5.2 Moving wire

On the unshielded MKE-L8 kicker moving wire measurements were done. The longitudinal impedance was evaluated with horizontal offsets of up to ± 20 mm and vertical offsets up to ± 15 mm in steps of 5 mm. A typical sample of raw data is plotted

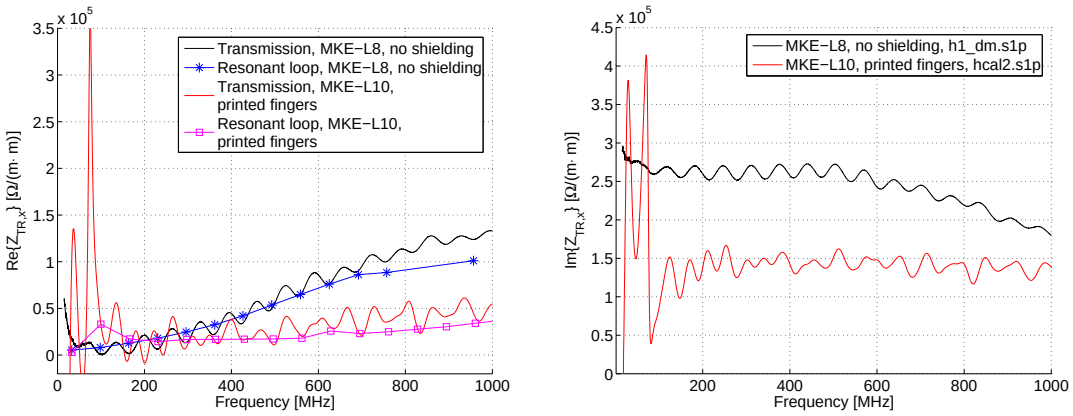

(a) (b) Imaginary part

Figure 5.1: The horizontal Z_{TR} of an unshielded and a shielded MKE kicker as measured using the transmission and the resonant technique. Shielding decreases $Z_{TR,x}$ except at frequencies below 200 MHz.

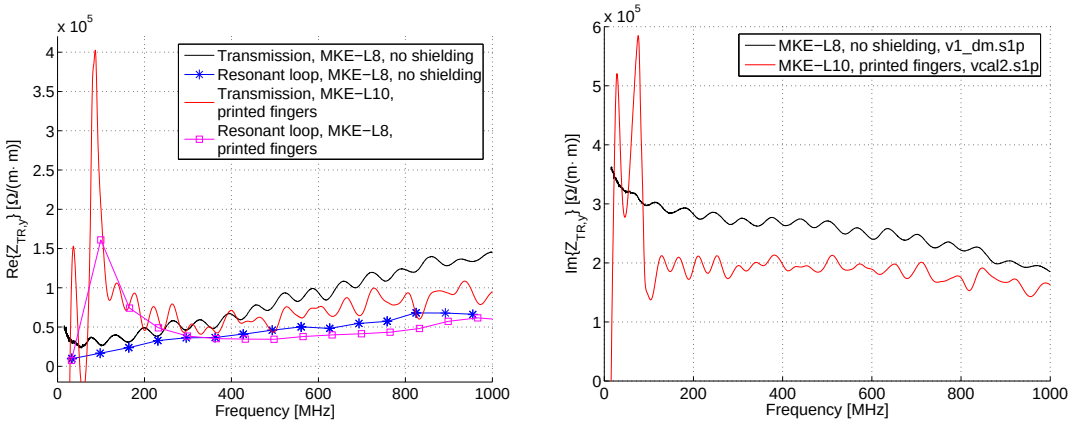

(a) (b)

Figure 5.2: The vertical Z_{TR} of an unshielded and a shielded MKE kicker. An enhanced Z_{TR} was found below 200 MHz with shielding and an impedance reduction above.

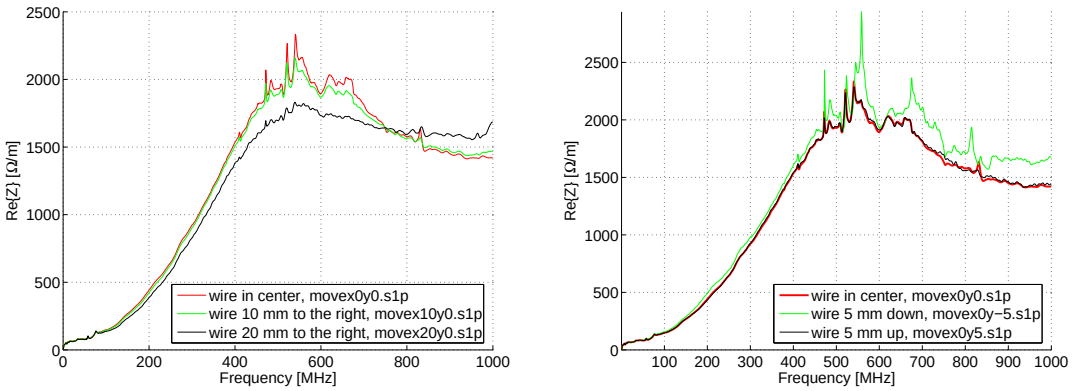

(a) Wire displaced horizontally.

(b) Wire displaced vertically

Figure 5.3: Moving wire measurements on the unshielded MKE-L8 kicker.

in Fig. 5.3. For horizontal movements the measured longitudinal impedance Z_m was found to decrease as the wire is moved off-center.

Fig. 5.4 and 5.5 show Z_m as a function of wire offset and frequency. The data was normalized to Z, i.e. the trace with zero offset. For horizontal displacements the parabola opens downward and for vertical displacements upward, corresponding to a negative Z_x and positive Z_y.

The values obtained by fitting for the "generalized" transverse impedance Z_x are shown in Fig. 5.6. It can be seen that the fitting procedure is robust: the resulting Z_x does not depend much on original data set. Very similar results are obtained when taking the full data set (9 points, offsets from -20 to $+20$ mm) or only a subset (5 points, offsets from -10 to $+10$ mm. Therefore the obtained results should be very reliable.

Fig. 5.7 depicts the fitting results for Z_y. For different data sets the outcome may vary considerably, indicating rather large uncertainties. These uncertainties are probably due to mechanical tolerances and sag. Above 500 MHz the fitting gives questionable results due to the presence of tank modes. For further evaluation the green trace was chosen as the most likely result, since the fitting yielded a parabola center in the correct range.

Calculating the sum $Z_x + Z_y = Z_{TR,x} + Z_{TR,y}$ the moving wire data can be compared with ordinary two wire data. The results are plotted in Fig. 5.8. For the imaginary part there is a rough agreement, while there are quite some discrepancies for the real part. The main source of uncertainty is the fitting of Z_y.

5.3 Summary

The impact of the MKE kicker shielding to reduce beam-induced heating on the transverse impedance was examined. Three different methods were used to determine Z_{TR} of an unshielded and a fully shielded kicker. In both planes a reduction of Z_{TR} was found above 200 MHz, while there was an increase below. The agreement between two wire transmission measurements and resonant measurements was good to acceptable, while a rough agreement was found between two wire and moving wire measurements. For

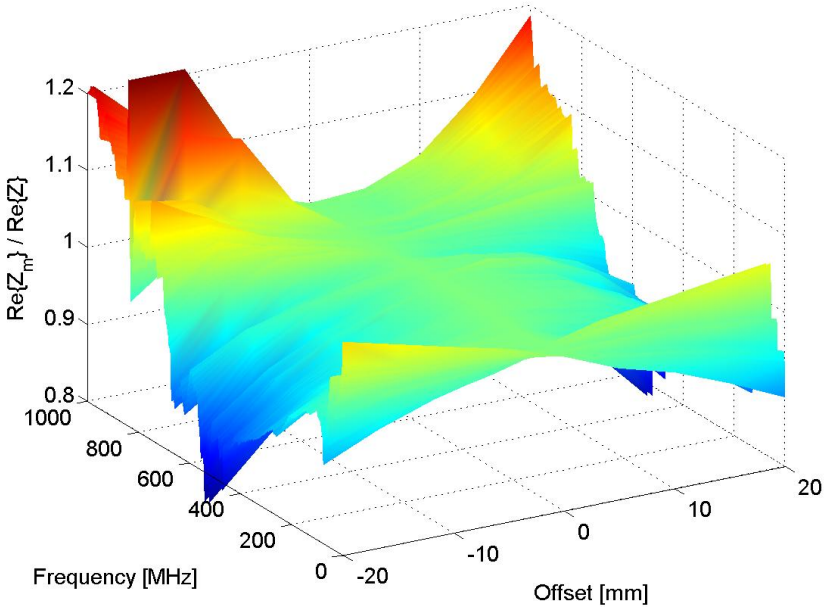

Figure 5.4: The impedance as a function of frequency and *horizontal* wire offset. The data was normalized to the zero-offset trace for ease of display. The parabola opens downwards, which indicates that the "generalized" transverse impedance Z_x is negative.

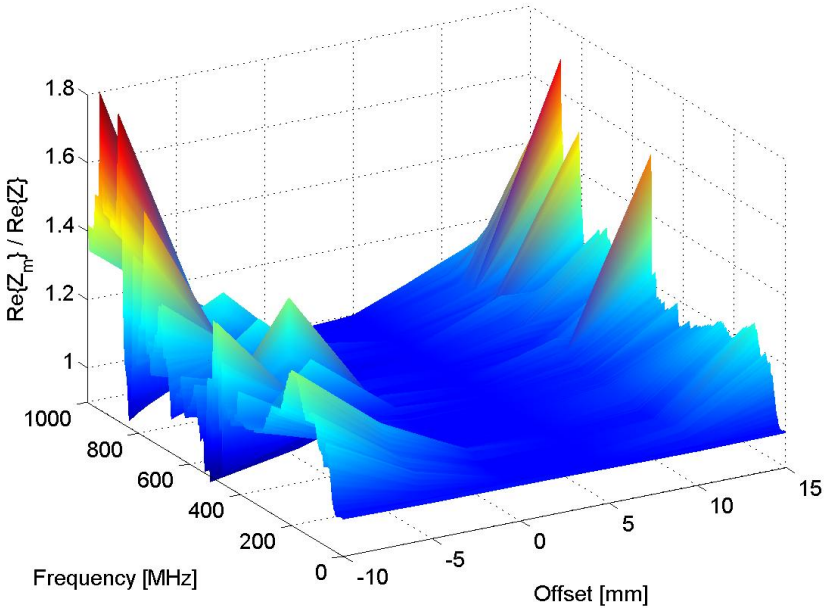

Figure 5.5: The impedance as a function of frequency and *vertical* wire offset. The data was normalized to the zero-offset trace for ease of display.

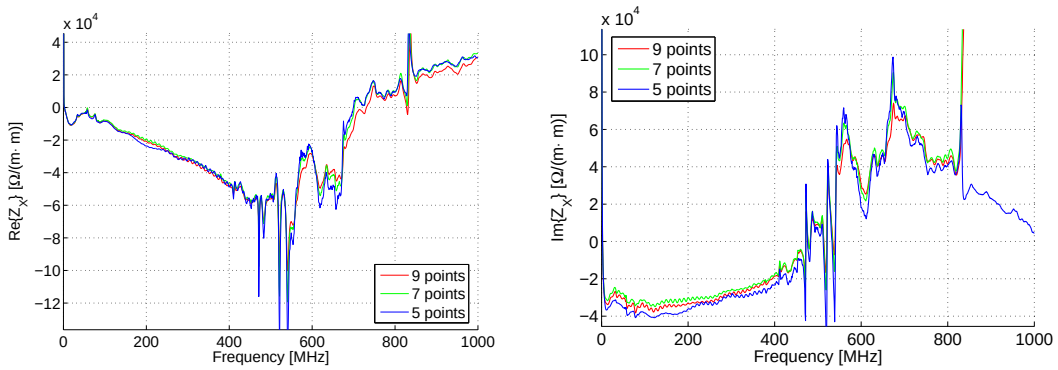

(a) (b)

Figure 5.6: The "generalized" horizontal transverse impedance Z_x calculated from the moving wire data. The results of the fitting do not depend much on the data set used, which indicates that they should be reliable.

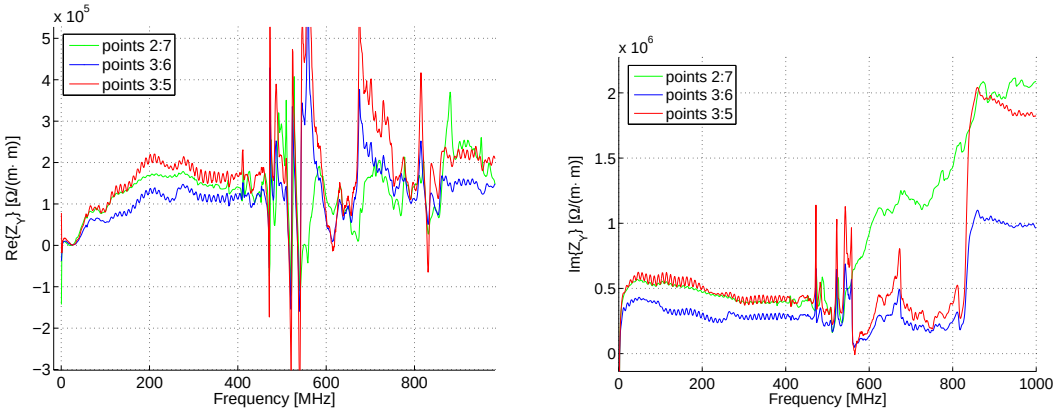

(a) (b)

Figure 5.7: The "generalized" vertical transverse impedance Z_y calculated from the moving wire data. Depending on the data set used the results vary considerably, which points to a rather large uncertainty.

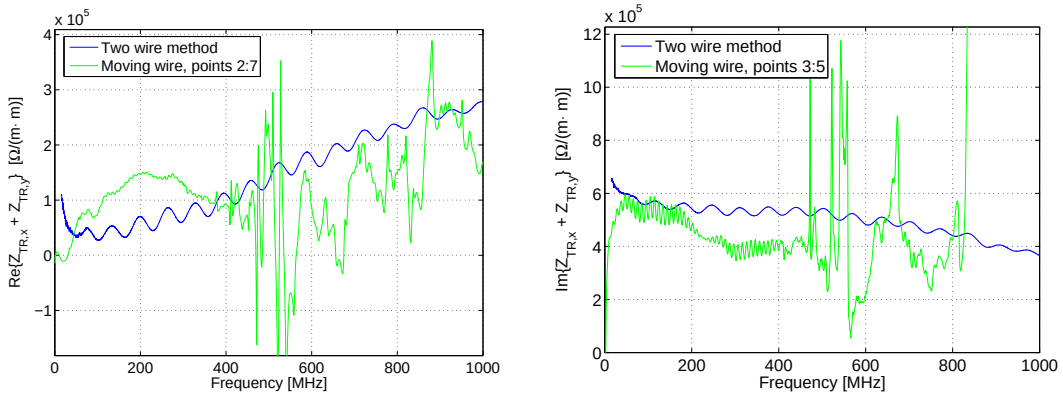

(a) (b)

Figure 5.8: Comparison of the two-wire transmission data and the moving wire data for MKE-L8. The discrepancies should be mainly due to mechanical uncertainties which affect the fitting of Z_y.

measurements in the vertical plane the main source of uncertainty is probably related to wire sag.

Conclusion

After the observation of substantial heating of the MKE kickers in 2003, it was decided to further study means to reduce the longitudinal kicker impedance. Several techniques for shielding the ferrite from the beam-induced magnetic fields were examined. First single ferrite cells were equipped with shielding and its efficiency evaluated in bench measurements applying the wire method. The most promising technique was identified as interleaved metallic fingers directly printed on the ferrite. Subsequently an entire magnet was equipped with shielding and subjected to impedance measurements. A reduction in heating by a factor four was obtained for LHC type beam. At the end of the 2006 SPS run strong indications of reduced heating in the first installed kicker with partial shielding were observed [27].
In order to reliably quantify the low remaining longitudinal impedance the measurement methods had to be optimized and new measurement techniques applied. The transverse impedance of shielded and unshielded kickers was assessed by three different methods, including a new resonant technique. It was found that the shielding has a positive effect above 200 MHz, while at lower frequencies an increase in transverse impedance was found, which is probably due to resonances related to the finger geometry.

Acknowledgements

We would like to thank the all the colleges of the AB-BT group who contributed to the above work. Thanks to Flemming Pedersen, Elena Shaposhnikova and Trevor Linnecar for support.

Bibliography

[1] Uythoven, J. et al., *Status report on beam induced heating of the MKE magnet*, http://ab-div.web.cern.ch/ab-div/Meetings/APC/2003/apc240603/uythoven.pdf (2003)

[2] Zimmermann, F., *Update on SPS impedance localization*, ab-div.web.cern.ch/ab-div/Meetings/APC/2006/apc060413/FZ-APC13-04-06.ppt (2006)

[3] Caspers, F., *Impedance Determination*, in: *Handbook of Accelerator Physics and Engineering*, World Scientific (1999)

[4] Meinke, H. and Gundlach, F. W., *Taschenbuch der Hochfrequenztechnik*, Dritte Auflage, Springer-Verlag, Berlin (1968), in German

[5] Hahn, H., Blaskiewicz, M., Davino, D., *Coupling Impedance Measurements of the SNS RF Cavity and Extraction Kicker Magnet*, PAC 2003, Portland (2003)

[6] Davino, D., Hahn, H., Lee, Y. Y., *Measurements of the Coupling Impedance of the SNS Extraction Kickers*, EPAC 2002, Paris (2002)

[7] Hahn, H., Pedersen, F., BNL 50870 (1978)

[8] Jensen, E., *An improved log-formula for homogeneously distributed impedance*, CERN-PS-RF-Note-2000-001, Geneva (2000)

[9] Hahn, H., *Validity of coupling impedance bench measurements*, Physical Review Special Topics - Accelerators and Beams, Volume 3, 122001 (2000)

[10] Bray, J. R. and Roy, L., *Measuring the unloaded, loaded, and external quality factors of one- and two-port resonators using scattering-parameter magnitudes at fractional power levels*, IEE Proc.-Microw. Antennas Propag., Vol. 151, No. 4, (2004)

[11] Fontolliet, P.-G., *Systemes de Telecommunications*, Traite d'Electricite, Vol. 17, Lausanne (1999), in French

[12] Tsutsui, H., *On single wire technique for transverse coupling impedance measurement*, CERN-SL-Note-2002-034-AP, Geneva, (2002)

[13] Nassibian, G., Sacherer, F., *Methods for measuring transverse coupling impedances in circular accelerators*, Nucl. Instrum. Methods 159 (1979)

[14] Caspers, F., Iriso-Ariz, U., Mostacci, A., *Bench Measurements of Low Frequency Transverse Impedance*, CERN-AB-2003-051-RF, Geneva (2003)

[15] Zinke, H. and Brunswig, H., *Lehrbuch der Hochfrequenztechnik*, Springer-Verlag, Berlin (1973), in German

[16] Metral, E. et al., *Kicker impedance measurements for the future multiturn extraction of the CERN Proton Synchrotron*, EPAC'06, Edinburgh, CERN-AB-2006-051 (2006)

[17] Ferroxcube, *Soft Ferrites and Accessories*, http://www.ferroxcube.com/ (2005)

[18] *The LHC Injector Chain*, LHC Design Report, Vol. 2, CERN-2004-003, Geneva (2004)

[19] Gaxiola, E. et al., *The Fast Extraction Kicker System In SPS LSS6*, LHC Project Report 913, Geneva (2006)

[20] Gaxiola, E., et al., *Experience with Kicker Beam Coupling Reduction Techniques*, CERN-AB-2005-024, Geneva (2005)

[21] Caspers, F., Mostacci, M. and Tsutsui, H., *Impedance Evaluation of the SPS MKE Kicker with Transition Pieces between Tank and Kicker Module*, CERN-SL-2000-071 (AP), Geneva (2000)

[22] Caspers, F., Gonzalez, C., Dyachkov, M., Shaposhnikova, E., Tsutsui, H., *Impedance measurement of the SPS MKE kicker by means of the coaxial wire method*, CERN-PS-RF-Note-2000-04, Geneva (2000)

[23] Caspers, F., *SPS Kicker Impedance Measurement and simulation*, Chamonix workshop 2000, sl-div.web.cern.ch/sl-div/publications/chamx2k/PAPERS/3_5.pdf, CERN, Geneva (2000)

[24] Hoffmann, R.K., *Integrierte Mikrowellenschaltungen*, Springer, Berlin (1983), in German

[25] Uythoven, J., Private communication (2006)

[26] Shaposhnikova, E., *SPS impedance and intensity limitations*, in: 1st CARE-HHH-APD Workshop on Beam Dynamics in Future Hadron Colliders and Rapidly Cycling High-Intensity Synchrotrons HHH 2004, CERN, Geneva (2004)

[27] Gaxiola, E., *SPS kicker temperature and vacuum monitoring data during beam scrubbing*, http://ab-div.web.cern.ch/ab-div/Meetings/APC/2006/apc060915/EG-APC-15-09-2006.pdf (2006)